Electrostatic stability of electron-positron plasmas in dipole geometry

Alexey Mishchenko[1]†, Gabriel G. Plunk[1] and Per Helander[1]

[1]Max Planck Institute for Plasma Physics, D-17491 Greifswald, Germany

(Received xx; revised xx; accepted xx)

The electrostatic stability of electron-positron plasmas is investigated in the point-dipole and Z-pinch limits of dipole geometry. The kinetic dispersion relation for sub-bounce-frequency instabilities is derived and solved. For the zero-Debye-length case, the stability diagram is found to exhibit singular behavior. However, when the Debye-length is non-zero, a fluid mode appears, which resolves the observed singularity, and also demonstrates that both the temperature and density gradients can drive instability. It is concluded that a finite Debye length is necessary to determine the stability boundaries in parameter space. Landau damping is investigated at scales sufficiently smaller than the Debye length, where instability is absent.

1. Introduction

The prospects of creating magnetically confined electron-positron (pair) plasmas in dipole or stellarator geometries have been discussed since early 2000's (Pedersen *et al.* 2003). In the near future, the first experiment will be constructed to confine such plasmas in magnetic dipole geometry (Pedersen *et al.* 2012). Recently, efficient injection and trapping of a cold positron beam in a dipole magnetic field configuration has been demonstrated by Saitoh *et al.* (2015) using a supported permanent magnet. This result is a key step towards the further studies using the levitated magnetic coil with the ultimate aim of creating and studying the first man-made magnetically-confined pair plasma in the laboratory.

It has been shown by Helander (2014) that pair plasmas possess unique stability properties due to the mass symmetry between the particle species. For example, drift instabilities are completely absent in straight-field-line geometry, e. g. in a slab, provided that the temperature and density profiles of the two species are equal ("symmetric" pair plasmas). The symmetry between the species is broken if the temperature profiles of the electrons and positrons differ or there is an ion contamination. Then, the drift instabilities can be excited (Mishchenko *et al.* 2017) even in unsheared slab geometry. In a sheared slab, pure pair plasmas are prone to current-driven reconnecting instabilities (Zocco 2017), although asymmetry between the species is also needed in this case since the ambient electron flow velocity must differ from the positron one for the ambient current to be finite. In contrast to slab geometry, a dipole magnetic field has finite curvature. In this case, the symmetry between the species is broken by the curvature drifts and the plasma is driven unstable by the temperature and density gradients (Helander 2014), even without ion contamination and for identical temperature profiles of the two species. This result persists also in the electromagnetic regime (Helander & Connor 2016). The nonlinear stability of dipole pair plasmas has also been addressed recently by (Helander 2017).

† Email address for correspondence: alexey.mishchenko@ipp.mpg.de

In this paper, we extend the results of Helander (2014) by performing a detailed study of the drift-kinetic stability of pure pair plasma in dipole geometry, making use of both the Z-pinch and point-dipole limits, where the dispersion relation is derived and numerically solved. The structure of the paper is as follows. In §2, we introduce the magnetic dipole field and discuss the near-magnetic-axis (Z-pinch) and far-field (point-dipole) limits. In §3, we introduce the linear drift-kinetic description and derive a "master" equation, applicable to both Z-pinch and point-dipole limits. The Z-pinch and point-dipole limits are then individually treated in §4 and §5, respectively. The conclusions are summarised in §6.

2. Dipole magnetic field

In cylindrical coordinates (r, φ, z), the magnetic field of a circular conducting loop with the radius r_0 carrying the total current I is

$$\mathbf{B}(r,z) = \nabla\psi(r,z) \times \nabla\varphi \ , \quad \nabla\varphi = \frac{\mathbf{e}_\varphi}{r} \tag{2.1}$$

with the poloidal magnetic flux given by (Landau & Lifshitz 1960; Simpson *et al.* 2001)

$$\psi(r,z) = \frac{C}{2}\sqrt{(r_0+r)^2+z^2}\left[\frac{r_0^2+r^2+z^2}{(r_0+r)^2+z^2}K(\kappa) - E(\kappa)\right] \ , \ C = \frac{\mu_0 I}{\pi} \tag{2.2}$$

defined in terms of the elliptic integrals of the first and the second kind:

$$K(k) = \int_0^1 \frac{\mathrm{d}x}{\sqrt{(1-x^2)(1-k^2x^2)}} \ , \ E(k) = \int_0^1 \frac{\sqrt{1-k^2x^2}}{\sqrt{1-x^2}}\,\mathrm{d}x \tag{2.3}$$

Following Simpson *et al.* (2001), we define

$$\kappa^2 = 1 - \rho^2/\beta^2 \ , \quad \rho^2 = (r-r_0)^2 + z^2 \ , \quad \beta^2 = (r_0+r)^2 + z^2. \tag{2.4}$$

The components of the magnetic field are then expressed

$$B_r = \frac{Cz}{2\rho^2\beta r}\left[(r_0^2+r^2+z^2)E(\kappa^2) - \rho^2 K(\kappa^2)\right] \tag{2.5}$$

$$B_z = \frac{C}{2\rho^2\beta}\left[(r_0^2-r^2-z^2)E(\kappa^2) + \rho^2 K(\kappa^2)\right] \tag{2.6}$$

We will consider two asymptotic cases of this magnetic geometry, depicted in Fig. 1. The first case arises in the region close to the current loop. This is the Z-pinch limit, corresponding to

$$\frac{r-r_0}{r_0} \sim \frac{z}{r_0} \sim \frac{\rho}{r_0} \ll 1. \tag{2.7}$$

In this case, $\beta \approx 2r_0$ so that $\kappa \to 1$ (Gradshteyn & Ryzhik 1980) and

$$E(\kappa) \approx 1 \ , \ \ K(\kappa) \approx \ln\left(\frac{4}{\sqrt{1-\kappa^2}}\right) \approx -\ln\left(\frac{\rho}{8r_0}\right) \tag{2.8}$$

Substituting these relations into Eqs. (2.5) and (2.6), we obtain

$$B_r \approx \frac{Cz}{2\rho^2} \ , \ \ B_z \approx -\frac{C(r-r_0)}{2\rho^2} \ , \ \ \psi = -\frac{Cr_0}{2}\ln\left(\frac{\rho}{8r_0}\right) \tag{2.9}$$

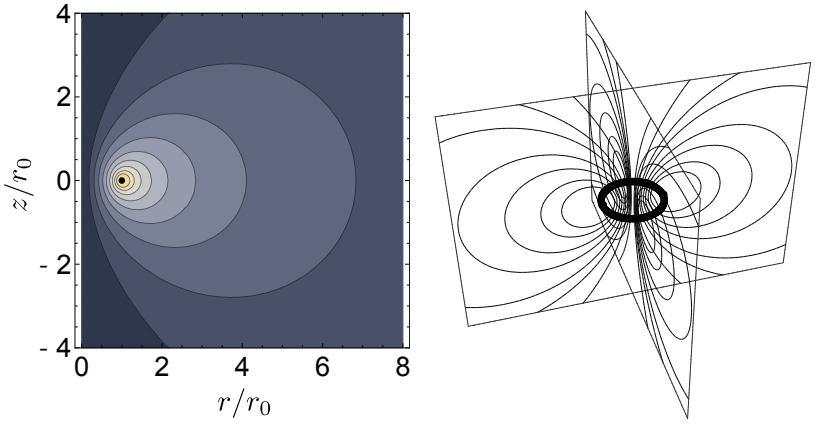

Figure 1: On the left is a plot of $\psi(r,z)$, as defined in Eqn. 2.2. Magnetic field lines (here, represented by contours of constant ψ) are generated by the circular coil at $(r,z)=(r_0,0)$, whose cross section is shown here as a small black disk. In the yellow region, close to the coil, the field is approximately that of a Z-pinch, whereas in the grey region, far from the coil, it approaches the field of a point dipole. On the right is a 3D cartoon of a dipole magnetic field.

Here, we employed $\rho \ll r_0$ and invoked

$$\lim_{x\to 0} x\ln x = 0 \;\Rightarrow\; \frac{\rho}{r_0}\,\ln\left(\frac{\rho}{r_0}\right) \ll 1 \tag{2.10}$$

Introducing a new "quasi-polar" coordinate system, with the axis corresponding to the magnetic axis (the current loop), we define the new "quasi-polar" angle ζ satisfying

$$\sin\zeta = \frac{z}{\rho}\;,\;\; \cos\zeta = \frac{r-r_0}{\rho}\;,\;\; \mathbf{e}_\zeta = \frac{\nabla\zeta}{|\nabla\zeta|} = -\,\mathbf{e}_r\sin\zeta + \mathbf{e}_z\cos\zeta \tag{2.11}$$

In these notations, the magnetic field becomes

$$B_r = \frac{\mu_0 I}{2\pi\rho}\sin\zeta\;,\;\; B_z = -\,\frac{\mu_0 I}{2\pi\rho}\cos\zeta\;,\;\; \mathbf{B} = -\,\frac{\mu_0 I}{2\pi\rho}\,\mathbf{e}_\zeta \tag{2.12}$$

This is the usual Z-pinch magnetic field, created by a linear current flowing in the axial direction.

The second case to be considered corresponds to the far-field limit. For this case, the spherical coordinate system $(\hat r,\hat\theta,\varphi)$, with $\hat r$ the spherical radial distance, $\hat\theta$ the azimuthal angle, and φ the polar angle, is more convenient. For $\hat r \gg r_0$, the magnetic field is

$$B_r \approx \frac{2M\cos\hat\theta}{\hat r^3}\;,\;\; B_\theta \approx \frac{M\sin\hat\theta}{\hat r^3}\;,\;\; \psi = \frac{M\sin^2\hat\theta}{\hat r}\;,\;\; M = \frac{\mu_0 I r_0^2}{4} \tag{2.13}$$

These expressions are called the "point-dipole approximation", valid far from the current loop.

3. Drift-kinetic theory

Following Helander (2014) and Helander & Connor (2016), we begin with gyrokinetic theory. It is convenient to write the gyrokinetic distribution function in the form:

$$f_a = f_{a0}\left(1 - \frac{e_a\phi}{T_a}\right) + g_a = f_{a0} + f_{a1}\ , \quad f_{a1} = -\frac{e_a\phi}{T_a} f_{a0} + g_a \tag{3.1}$$

Here, f_{a0} is a Maxwellian, a is the species index with $a = e$ corresponding to the electrons, $a = p$ to the positrons. The linearised gyrokinetic equation in this notation is

$$iv_\parallel \nabla_\parallel g_a + (\omega - \omega_{\mathrm{d}a}) g_a = \frac{e_a}{T_a} J_0\left(\frac{k_\perp v_\perp}{\omega_{ca}}\right)\left(\omega - \omega_{*a}^T\right)\phi\, f_{a0} \tag{3.2}$$

with J_0 the Bessel function, ω_{ca} the cyclotron frequency, $k_\perp$ the perpendicular wave number, and ϕ the perturbed electrostatic potential. The notation used is summarized as follows:

$$\omega_{*a}^T = \omega_{*a}\left[1 + \eta_a\left(\frac{v^2}{v_{\mathrm{th}a}^2} - \frac{3}{2}\right)\right]\ , \quad v = \sqrt{v_\parallel^2 + v_\perp^2}\ , \quad \mu = \frac{m_a v_\perp^2}{2B} \tag{3.3}$$

$$\omega_{*a} = \frac{k_\varphi T_a}{e_a}\frac{\mathrm{d}\ln n_a}{\mathrm{d}\psi}\ , \quad \eta_a = \frac{\mathrm{d}\ln T_a}{\mathrm{d}\ln n_a}\ , \quad v_{\mathrm{th}a} = \sqrt{\frac{2T_a}{m_a}}\ , \quad \omega_{ca} = \frac{e_a B}{m_a} \tag{3.4}$$

$$\omega_{\mathrm{d}a} = \mathbf{k}_\perp \cdot \mathbf{v}_{\mathrm{d}a}\ , \quad \mathbf{v}_{\mathrm{d}} = \left(mv_\parallel^2 + \mu B\right)\frac{\mathbf{b}\times\nabla B}{qB^2}\ , \quad \mathbf{k}_\perp = k_\psi \nabla\psi + k_\varphi \nabla\varphi \tag{3.5}$$

Here, ψ is the poloidal flux and φ is the polar (toroidal) angle. We choose the sign convention such that $\omega_{*e} \geqslant 0$ for the electrons and $\omega_{*p} \leqslant 0$ for the positrons. We will assume the drift-kinetic limit in what follows, *i.e.* $k_\perp v_{\mathrm{th}a}/\omega_{ca} \ll 1$ so $J_0 \approx 1$.

Applying the bounce average to Eqn. 3.2, we obtain to lowest order

$$(\omega - \overline{\omega}_{\mathrm{d}a}) g_a = (\omega - \omega_{*a}^T)\frac{e_a\overline{\phi}}{T} f_{a0}, \tag{3.6}$$

with the bounce-average operation defined as

$$\overline{(\ldots)} = \oint (\ldots)\frac{\mathrm{d}l}{v_\parallel} \Big/ \oint \frac{\mathrm{d}l}{v_\parallel}. \tag{3.7}$$

Here, l is the arc length measured along a magnetic field line and the integration is performed between bounce points for trapped particles, and over the entire closed field line for passing particles. Note that there are only trapped particles in the point-dipole limit and only passing particles in the Z pinch limit. We assume the temperature and the density profiles of the electrons and the positrons to be identical, and invoke the Poisson equation:

$$\left(\sum_{a=e,p}\frac{n_a e_a^2}{T_a} + \epsilon_0 k_\perp^2\right)\phi = \sum_{a=e,p} e_a \int g_a \mathrm{d}^3 v\ , \tag{3.8}$$

We find that the perturbed electrostatic potential satisfies the equation:

$$\left(1 + k_\perp^2 \lambda_D^2\right)\phi = \frac{1}{n_0}\int \frac{\omega^2 - \overline{\omega}_d \omega_*^T}{\omega^2 - \overline{\omega}_d^2}\overline{\phi}\, f_0 \mathrm{d}^3 v \tag{3.9}$$

Here and in the following, we use the notation $\omega_*^T \equiv \omega_{*e}^T$, $\omega_* \equiv \omega_{*e}$, $\overline{\omega}_d \equiv \overline{\omega}_{\mathrm{d}e}$, $n_0 = n_e$, $T_0 \equiv T_e$, and the Debye length is defined as usual $\lambda_D = \sqrt{\epsilon_0 T_0/(2n_0 e^2)}$.

Eq. (3.9) is the "master" equation for drift-kinetic stability in magnetic dipole geometry. It will be solved in Z-pinch and point-dipole limits. This will give us insight into the general properties of the stability of symmetric pair plasmas in magnetic dipole geometry.

4. Z-pinch case

In the Z-pinch limit, the components (in polar coordinates) of the magnetic field and the perpendicular wave vector, i. e. $\mathbf{B}\cdot\mathbf{e}_\zeta$ and $\mathbf{k}_\perp\cdot\mathbf{e}_\zeta$, etc. are flux functions. In this case, there is no particle trapping, and the orbit average of the perturbed electrostatic potential $\bar{\phi}$ coincides with its field-line average $\langle\phi\rangle$

$$\langle\phi\rangle = \oint \phi\,\mathrm{d}l \Big/ \oint \mathrm{d}l \tag{4.1}$$

Taking the field-line average of Eq. (3.9), one can perform the velocity integrals appearing there analytically following Biglari *et al.* (1989). This results in

$$1+k_\perp^2\lambda_D^2 = \frac{1}{2}(D_+ + D_-)\ ,\quad D_\pm = \frac{1}{\sqrt{\pi}}\int \frac{\Omega \mp \Omega_*^T}{\Omega \mp x_\perp^2/2 \mp x_\parallel^2}\,\exp(-x^2)\,x_\perp \mathrm{d}x_\perp \mathrm{d}x_\parallel \tag{4.2}$$

where we write $\omega_d = \hat{\omega}_d(x_\parallel^2 + x_\perp^2/2)$, $\Omega = \omega/\hat{\omega}_d$, $x = \sqrt{x_\parallel^2+x_\perp^2}$, $\Omega_*^T = \omega_*^T/\hat{\omega}_d = \Omega_*[1+\eta(x^2-3/2)]$, and $\Omega_* = \omega_*/\hat{\omega}_d$. Note that the function D_+ was obtained by Biglari *et al.* (1989), and here we generalize their calculation to obtain D_-, which arises because of the sign difference between the ion (positron here) and the (non-adiabatic) electron drifts. To compute this function, one can perform the same integrals, but with the complex frequency in the lower half plane. We find

$$D_\pm(\Omega) = Y_\pm^2 + \Omega_*\left\{\left[\pm\frac{\eta-1}{\Omega} - 2\eta\right]Y_\pm^2 \pm 2\eta Y_\pm\right\} \tag{4.3}$$

where

$$Y_+(\Omega) = \int_\infty^\Omega \frac{dz}{\sqrt{z}}\exp(z-\Omega) = -\sqrt{\Omega}Z(\sqrt{\Omega}), \tag{4.4}$$

$$Y_-(\Omega) = \int_{-\infty}^\Omega \frac{dz}{\sqrt{z}}\exp(\Omega-z) = \sqrt{\Omega}\left[2i\sqrt{\pi}\exp(\Omega) - iZ(-i\sqrt{\Omega})\right], \tag{4.5}$$

and Z is the plasma dispersion function. When $\mathrm{Im}[\Omega] > 0$, $\sqrt{\Omega}$ is defined as the principle root (which lies in the upper half plane). To treat Landau damping, $Y_\pm$ must be analytically continued to perform the contour integral in the inversion of the Laplace transform. In particular, we must choose the branch of $\sqrt{\Omega}$ so that the function remains analytic. Very closely related problems were treated by (Sugama 1999) and (Helander *et al.* 2011), who chose the branch cut of the function $\sqrt{\Omega}$ to lie along the negative imaginary axis. This approach allows pole contributions to be picked up in the usual fashion, with an additional contribution coming from integration along the branch cut; see Fig. 2.

In the present case we take a different approach, namely to perform the integral in the $\sqrt{\Omega}$ plane, in which it is possible to continue the dispersion function analytically over the entire plane, avoiding the need for a branch cut. The reason for this choice is that the pole contributions can cross the negative imaginary axis, and therefore evade detection; a case where this happens is shown in Fig. 3. The new contour for Laplace inversion is shown Fig. 4. In this figure, the curved paths are contours of constant $\mathrm{Im}[\Omega]$. Thus, the standard curve for inverting a Laplace transform is shown in dashed blue. The new contour is chosen so that it lies in the upper left and lower right quadrants, where $\mathrm{Im}[\Omega] < 0$. The curved portions of the path can be neglected as compared to the pole contributions, for the usual reason that the corresponding part of the solution is damped more strongly than the pole contributions.

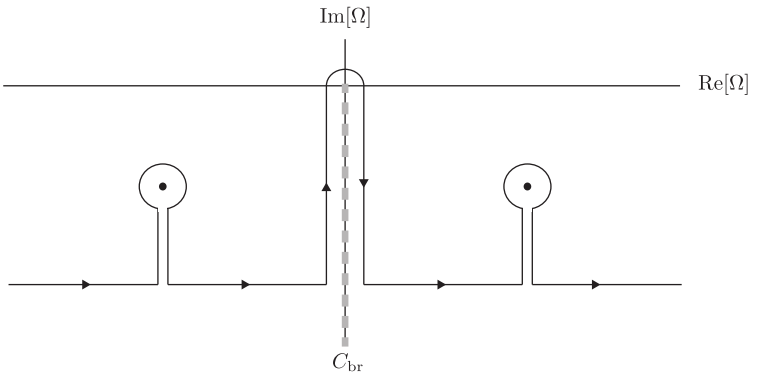

Figure 2: Landau contour appearing in Refs. (Sugama 1999) and (Helander *et al.* 2011). The branch cut is the grey dashed line labeled as $C_{\rm br}$.

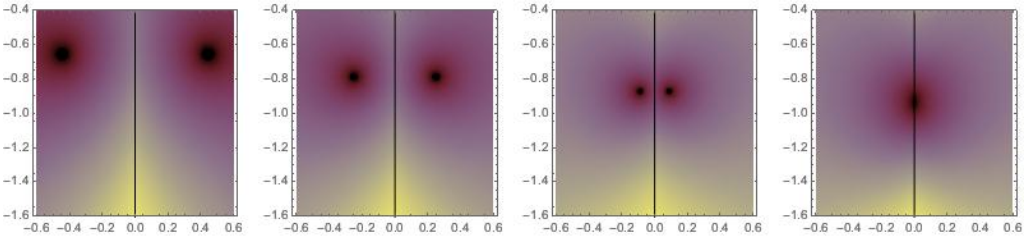

(a) Symmetrized case: branch cut of $\sqrt{\Omega}$ lies on negative imaginary axis. Both poles present until they cross the branch cut and are lost.

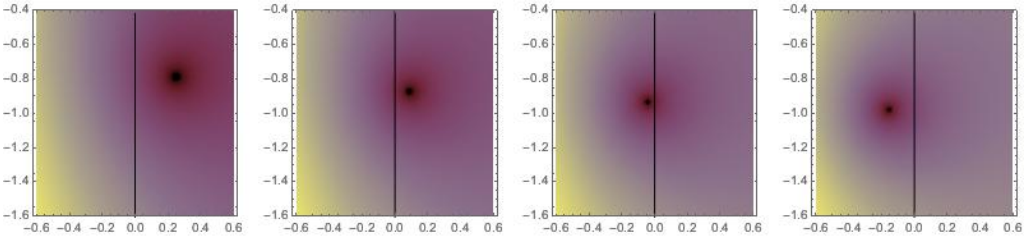

(b) With branch cut of $\sqrt{\Omega}$ placed on negative real axis, one pole can be found.

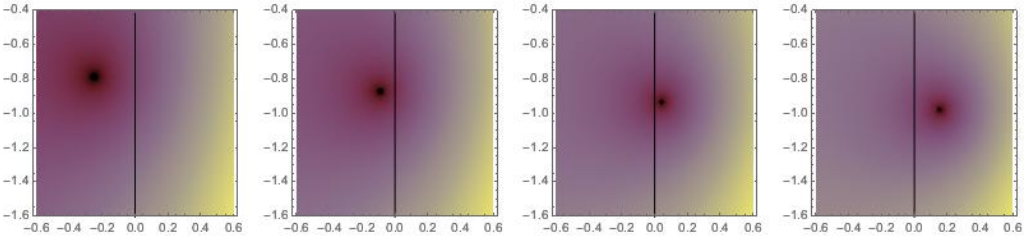

(c) With branch cut of $\sqrt{\Omega}$ placed on positive real axis, one pole can be found.

Figure 3: Density plot of dispersion function $1 + k_\perp^2\lambda_D^2 - (D_+ + D_-)/2$ in the complex Ω plane. Poles are observed to cross the negative imaginary axis as $k_\perp^2\lambda_D^2$ is varied. Here $\eta = 10$, $\Omega_* = 1$, and the values of $k_\perp^2\lambda_D^2$ are 6, 8, 10 and 12.

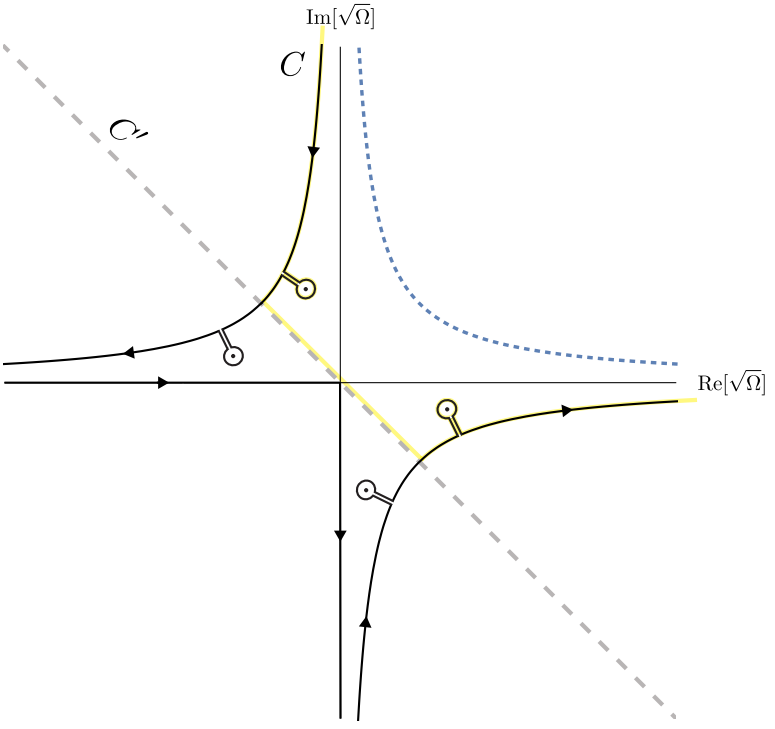

Figure 4: Extended Landau contour, C. Note that the negative imaginary Ω axis is mapped to the grey dashed line, labeled C', and the contour of Fig. 2 is shown in light yellow for comparison. Note that the path of Fig. 2 does not encircle the depicted poles that lie beneath C', which is why we use the modified contour here.

As was found by (Sugama 1999) and (Helander *et al.* 2011), part of the integral causes algebraic damping, while the pole contributions, *i.e.* the complex mode frequencies, can be obtained as the roots of Eq. (4.2). In the present case, the algebraic damping comes from the integral running along the negative $\mathrm{Re}[\sqrt{\Omega}]$ and $\mathrm{Im}[\sqrt{\Omega}]$ axes. The long-time limit of this contribution is dominated by the $\Omega \to 0$ point, and goes as $1/t^2$. We further note that this algebraic contribution correspond to integrals along the real axis in the Ω plane. Thus, the damping can be assured to be non-exponential, and any exponential damping comes explicitly from the identified poles.

In practice, the consequence of the above discussion is that the complex frequency of Landau-damped modes is determined by roots of the dispersion function $1 + k_\perp^2\lambda_D^2 - (D_+ + D_-)/2$ that lie in either the upper-left and lower-right quadrant in the complex $\sqrt{\Omega}$ plane. Landau damping will occur at sufficiently large values of $k_\perp\lambda_D$.

At $k_\perp\lambda_D \lesssim 1$, the fluid limit $\Omega \gg 1$ can be applied to Eq. (4.2), yielding the solution

$$\omega^2 = -\frac{\hat{\omega}_d^2}{k_\perp^2\lambda_D^2}\left[(1+\eta)\frac{\omega_*}{\hat{\omega}_d} - \frac{7}{4}\right]. \tag{4.6}$$

Note that the temperature and density gradients act together (via the factor $1+\eta$), and a purely density-gradient-driven mode is possible, unlike the related interchange instability in a conventional electron-ion plasma. The mode is predicted to be stabilized when $\hat{\omega}_d$ exceeds ω_*. This results in the "fluid" instability condition (which is the singularity boundary if $k_\perp\lambda_D = 0$ exactly):

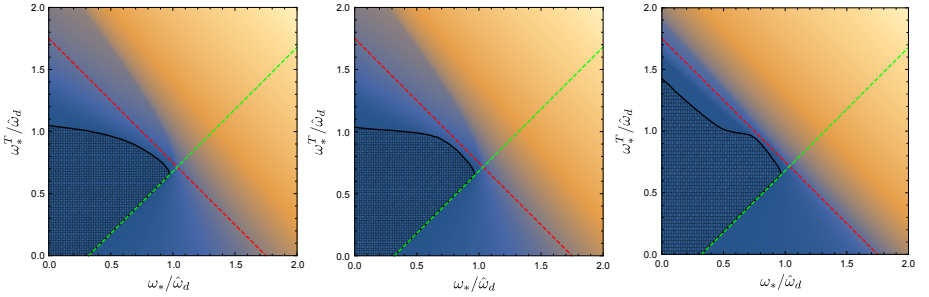

(a) $k_\perp^2\lambda_D^2 = 0.01$ (b) $k_\perp^2\lambda_D^2 = 0.0025$ (c) $k_\perp^2\lambda_D^2 = 0.000625$

Figure 5: Stability diagram for several values of $k_\perp^2\lambda_D^2$, compared with theoretical stability boundaries. The colour of the density plot corresponds to numerically obtained growth rate (dark blue is zero and large positive values are yellow). The region of absolute stability is darkened and bordered by a solid black contour. The theoretical stability lines (dashed red, and dashed green) correspond respectively to Eqs. (4.7) and (4.9). Note that the deviation from the red theoretical stability boundary (which does not include finite-$k_\perp\lambda_D$ corrections) decreases as $k_\perp^2\lambda_D^2 \to 0$, though surprisingly slowly.

$$\frac{\omega_*}{\hat{\omega}_d}(1+\eta) > \frac{7}{4}. \tag{4.7}$$

Note, however, that the threshold condition $\omega = 0$ contradicts the "fluid" assumption $\Omega \gg 1$ made above. It indicates that higher-order terms may be needed to treat the plasma stability at the "fluid stability boundary" (singularity boundary for $k_\perp\lambda_D = 0$). Even when ω_* exceeds $\hat{\omega}_d$ sufficiently for the existence of an unstable "fluid" mode, the mode must succumb to Landau damping for sufficiently large $k_\perp\lambda_D$. We can take $\Omega \sim 1$ to estimate the wavenumber where this transition must occur:

$$k_\perp\lambda_D \sim \left|\frac{7}{4} - (1+\eta)\frac{\omega_*}{\hat{\omega}_d}\right|^{1/2} \tag{4.8}$$

For values of $k_\perp\lambda_D$ exceeding this, we return to the Landau damping problem.

We can also derive the "resonant stability boundary" taking $\Omega \to 0$ in Eq. (4.2), obtaining

$$\frac{\omega_*}{\hat{\omega}_d}(1-\eta) = \frac{1+k_\perp^2\lambda_D^2}{\pi}. \tag{4.9}$$

As it turns out, the true stability boundary runs along portions each of the two stability boundaries, Eqs. (4.7) and (4.9), as demonstrated in Fig. 5.

5. Point dipole case

Now we turn to dipole geometry. In contrast to the Z-pinch limit, the magnetic field strength and perpendicular wave vector change along field lines in the dipole geometry, i. e. $B = B(\psi, l)$ and $k_\perp = k_\perp(\psi, l)$, *etc.*, depend on ψ the poloidal flux and l the distance measured along a field line. It has been shown by Kessner & Hastie (2002) that the bounce-averaged drift frequency in the point dipole can be approximated with very good accuracy as $\overline{\omega}_d \approx 4k_\varphi mv^2/(3e\psi)$. Using this approximation, the integrals in

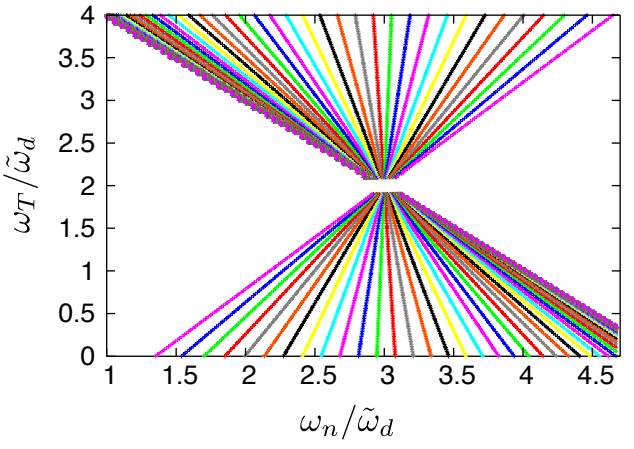

Figure 6: Contours of constant growth rate γ plotted in the two-dimensional parameter space (ω_n, ω_T). The diamagnetic frequencies ω_n and ω_T are normalised to the drift frequency $\tilde{\omega}_d$. Different colours indicate different values of γ. The density of the contours shows how fast the growth rate changes. Note that this density is especially high near the "singularity boundary", defined in Eq. (5.7).

Eq. (3.9) can be factorised into velocity (v) and pitch-angle (λ) parts:

$$\left(1 + k_\perp^2 \lambda_D^2\right)\phi = \Lambda \int_0^{1/B} \frac{B\mathrm{d}\lambda}{\sqrt{1-\lambda B}}\,\bar{\phi}\ , \quad \Lambda = \frac{1}{n_0}\int_0^\infty \frac{\omega^2 - \overline{\omega}_d\omega_*^T}{\omega^2 - \overline{\omega}_d^2}\, f_0\, 2\pi v^2 \mathrm{d}v \tag{5.1}$$

In this Section, we will focus on the growing solutions with $\gamma = -i\omega > 0$. To begin, we assume $k_\perp \lambda_D \to 0$ and employ the relations:

$$\oint \mathrm{d}l \int_0^{1/B} \frac{\mathrm{d}\lambda}{\sqrt{1-\lambda B}}\,\bar{\phi} = 2\oint \frac{\mathrm{d}l}{B}\,\phi\ , \quad \bar{\phi}(\lambda) = \frac{1}{\oint \frac{\mathrm{d}l}{\sqrt{1-\lambda B}}}\oint \frac{\phi\,\mathrm{d}l}{\sqrt{1-\lambda B}} \tag{5.2}$$

In this case, the dispersion relation is simply $\Lambda = 1/2$. Expressing the velocity integrals through the plasma dispersion function $Z_0(\zeta)$, we obtain

$$\Lambda = \frac{1}{2}\left[\frac{\omega_*\eta}{\omega\zeta}\overline{Z}_6(\zeta) + \frac{\omega_*}{\omega\zeta}\left(1 - \frac{3\eta}{2}\right)\overline{Z}_4(\zeta) - \zeta\overline{Z}_2(\zeta)\right]\ , \quad \tilde{\omega}_d = \frac{4k_\varphi T}{3e\psi} \tag{5.3}$$

$$\zeta = \sqrt{\frac{\omega}{2\tilde{\omega}_d}}\ , \quad \overline{Z}_n(\zeta) = Z_n(\zeta) + iZ_n(i\zeta)\ , \quad Z_n(\zeta) = \frac{1}{\sqrt{\pi}}\int_{-\infty}^{\infty}\frac{x^n e^{-x^2}\mathrm{d}x}{x-\zeta} \tag{5.4}$$

which leads to the dispersion relation

$$\frac{\omega_*\eta}{\omega\zeta}\overline{Z}_6 + \frac{\omega_*}{\omega\zeta}\left(1 - \frac{3\eta}{2}\right)\overline{Z}_4 - \zeta\overline{Z}_2 = 1 \tag{5.5}$$

Taking the limit $\zeta \to 0$, we find the "stability" boundary (Helander 2014):

$$\frac{\omega_n - \omega_T}{\tilde{\omega}_d} = 1.\ , \quad \omega_n = \omega_*\ , \quad \omega_T = \eta\omega_* \tag{5.6}$$

Taking the opposite limit $\zeta \to \infty$, we find the "singularity" boundary:

$$\frac{\omega_n + \omega_T}{\tilde{\omega}_d} = 5 \quad \Leftrightarrow \quad \frac{\mathrm{d}\ln(nT)}{\mathrm{d}\ln\psi} = \frac{20}{3} \tag{5.7}$$

Interestingly, the singularity boundary coincides with the MHD stability threshold (Helander & Connor 2016), although Eq. (5.7) has been obtained within the electrostatic formalism. Both the stability and the singularity boundaries can be seen in the numerical solution of the dispersion relation (5.5), shown in Fig. 6. Here, contours of constant growth rate γ are plotted in the two-dimensional parameter space (ω_n, ω_T). Different colours in Fig. 6 indicate different values of the growth rate. The density of the contours shows how fast the growth rate changes. One sees that the contour density is especially high near the singularity boundary. The numerical solutions of Eq. (5.5) in the domain bounded by Eqs. (5.6) and (5.7) represent all unstable modes with finite growth rates.

In Fig. 6, one sees a special point in the parameter space where the stability line $\omega_n - \omega_T = \tilde{\omega}_d$ crosses the singularity line $\omega_T + \omega_n = 5\,\tilde{\omega}_d$. The solution of this system of equations is $\omega_T = 2\,\tilde{\omega}_d$ and $\omega_n = 3\,\tilde{\omega}_d$. At this point $\eta = 2/3$ and $\omega_T/\omega = 1/\zeta^2$. The dispersion relation at the crossing point reduces to the expression:

$$\frac{\overline{Z}_6}{\zeta^3} - \zeta\overline{Z}_2 = 1 \tag{5.8}$$

We notice, however, that this expression is an identity, i. e. it is valid for all values of ζ, and can be derived from the definition of $\overline{Z}_n$. Thus it cannot be used to determine ζ. Nevertheless, one can simplify the dispersion relation by transforming the parameter-space coordinates (ω_n, ω_T) so that the origin coincides with the crossing point:

$$\frac{\omega_T}{\tilde{\omega}_d} = 2 + \tau \ , \quad \frac{\omega_n}{\tilde{\omega}_d} = 3 + \nu \ , \quad \eta = \frac{2+\tau}{3+\nu} \tag{5.9}$$

Written in these (ν, τ) parameters, the dispersion relation, Eq. (5.5) reduces to

$$\tau\overline{Z}_6 + \left(\nu - \frac{3\tau}{2}\right)\overline{Z}_4 = 0 \tag{5.10}$$

One sees that the contours of constant growth rate (i. e. constant ζ and therefore constant $\overline{Z}_6/\overline{Z}_4$) are indeed straight lines, in agreement with Fig. 6:

$$\frac{\nu}{\tau} = \frac{3}{2} - \frac{\overline{Z}_6}{\overline{Z}_4} \quad \Leftrightarrow \quad \tau = \left[\frac{3}{2} - \frac{\overline{Z}_6(\zeta)}{\overline{Z}_4(\zeta)}\right]^{-1} \nu \tag{5.11}$$

Using the identity Eq. (5.8), one can cast the dispersion relation Eq. (5.5) into an alternative form that is particularly simple :

$$\omega_T = c_\nu(\zeta)\omega_n + \Big[2 - 3c_\nu(\zeta)\Big]\tilde{\omega}_d \ , \quad c_\nu(\zeta) = \left[\frac{3}{2} - \frac{\overline{Z}_6(\zeta)}{\overline{Z}_4(\zeta)}\right]^{-1} \tag{5.12}$$

We stress that this formulation is equivalent to Eq. (5.5). Only the algebraic identity Eq. (5.8) and no additional assumptions were needed to derive it. The growth rate enters only through the coefficient $c_\nu(\zeta)$ which is plotted in Fig. 7. One sees that the asymptotic values of this coefficient are

$$\lim_{\zeta\to 0} c_\nu(\zeta) = 1 \ , \quad \lim_{\zeta\to\infty} c_\nu(\zeta) = -1 \tag{5.13}$$

It is straightforward to recover the stability and singularity boundaries from these values. The crossing point corresponds to the singularity of $c_\nu(\zeta)$, as shown in Fig. 7.

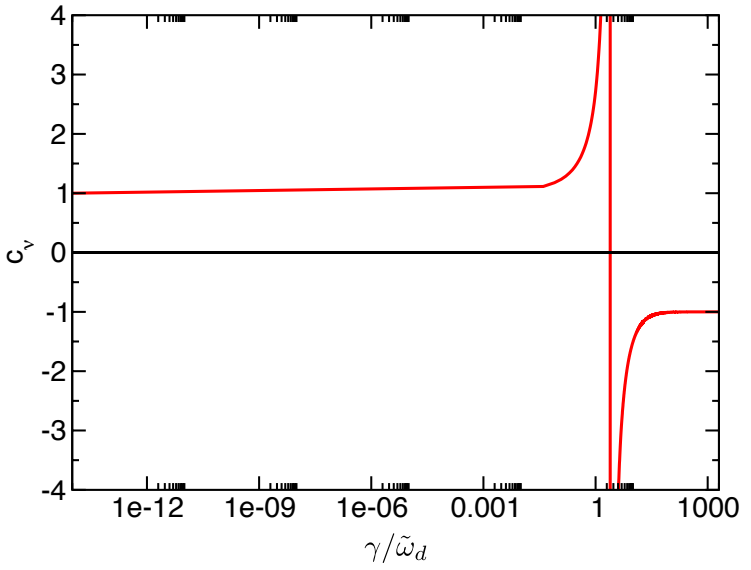

Figure 7: Frequency-dependent coefficient c_ν as a function of ζ.

5.1. *Finite Debye length*

From the preceding results it can be inferred that $k_\perp \lambda_D$ is a singular limit. Indeed Eq. (4.6) demonstrates the existence of a fluid mode whose growth rate varies inversely with $k_\perp \lambda_D$. Therefore, we will re-examine the point dipole limit, assuming a finite Debye length. This leads to a resolution of the singularity boundary that was encountered in the case where $k_\perp \lambda_D$ is taken to be exactly zero. We return to Eq. (5.1):

$$\left(1 + k_\perp^2 \lambda_D^2\right)\phi = \Lambda \int_0^{1/B} \frac{B \mathrm{d}\lambda}{\sqrt{1-\lambda B}}\, \bar{\phi}\ , \quad \Lambda = \frac{1}{n_0} \int_0^\infty \frac{\omega^2 - \overline{\omega}_d \omega_*^T}{\omega^2 - \overline{\omega}_d^2}\, f_0\, 2\pi v^2 \mathrm{d}v \tag{5.14}$$

Multiplying this equation with ϕ and integrating it over the field line $\oint \phi\, (\mathrm{d}l/B) \ldots$, we obtain the energy principle:

$$\oint \frac{\mathrm{d}l}{B} \left[(k_\perp \lambda_D)^2 \phi^2 + \int_0^{1/B} \frac{B \mathrm{d}\lambda}{\sqrt{1-\lambda B}} \left(\phi - \bar{\phi}\right)^2 \right] = \tag{5.15}$$

$$= \left(\Lambda - \frac{1}{2}\right) \oint \frac{\mathrm{d}l}{B} \int_0^{1/B} \frac{B \mathrm{d}\lambda}{\sqrt{1-\lambda B}}\, \bar{\phi}^2$$

This relation is general and has been derived without further assumptions other than neglecting the dependence of $\overline{\omega}_d$ on the pitch angle λ. It is convenient to obtain the stability condition in the fluid limit $\omega \to \infty$. In this limit

$$\Lambda - \frac{1}{2} \approx -\frac{3\,\tilde{\omega}_d^2}{2\omega^2} \left[\frac{\omega_T + \omega_n}{\tilde{\omega}_d} - 5 \right] \tag{5.16}$$

This can be reformulated into the stability condition in the fluid limit:

$$\omega^2 = -\frac{3\,\tilde{\omega}_d^2 \oint \frac{\mathrm{d}l}{B} \int_0^{1/B} \frac{B\mathrm{d}\lambda}{\sqrt{1-\lambda B}}\,\bar{\phi}^2}{2\oint \frac{\mathrm{d}l}{B}\left[(k_\perp\lambda_D)^2\phi^2 + \int_0^{1/B} \frac{B\mathrm{d}\lambda}{\sqrt{1-\lambda B}}\left(\phi-\bar{\phi}\right)^2\right]}\left(\frac{\omega_T+\omega_n}{\tilde{\omega}_d}-5\right) \tag{5.17}$$

One sees that the plasma is unstable above the singularity line $(\omega_T+\omega_n)/\tilde{\omega}_d > 5$ and the singularity in the growth rate, previously observed for $k_\perp\lambda_D = 0$, is removed. Note that a similar fluid-type instability was found in the Z pinch, see Eq. (4.7).

Interestingly, the energy principle can also be used to obtain another useful result. It follows from the energy principle that $\phi = \overline{\phi}$ if $k_\perp\lambda_D = 0$, implying $\langle\phi\rangle = \overline{\phi} = \phi$, i. e. $\partial\phi/\partial l = 0$. It is a consequence of the energy principle Eq. (5.15) and the dispersion relation $\Lambda = 1/2$, which we have previously shown to hold for $k_\perp\lambda_D = 0$, see Eq. (5.1). If $k_\perp\lambda_D$ is finite, but small, the deviation of ϕ from its bounce average or field-line average should also be small $\phi \approx \langle\phi\rangle \approx \overline{\phi}$. Introducing the splitting:

$$\phi = \langle\phi\rangle + \widetilde{\phi}\ ,\quad \left\langle\widetilde{\phi}\right\rangle = 0\ ,\quad \widetilde{\phi} \sim \mathcal{O}\left(k_\perp^2\lambda_D^2\right) \tag{5.18}$$

with $\langle\phi\rangle$ denoting the field-line average and $\widetilde{\phi}$ being small for $k_\perp\lambda_D \ll 1$, we can write Eq. (5.14) in the form:

$$\left(1+k_\perp^2\lambda_D^2\right)\langle\phi\rangle + \widetilde{\phi} + k_\perp^2\lambda_D^2\widetilde{\phi} = 2\Lambda\langle\phi\rangle + \Lambda\int_0^{1/B}\frac{B\mathrm{d}\lambda}{\sqrt{1-\lambda B}}\,\overline{\widetilde{\phi}} \tag{5.19}$$

Integrating this equation along the closed field line and taking into account that

$$\oint\frac{\mathrm{d}l}{B}\,\widetilde{\phi} = 0\ ,\quad \oint\frac{\mathrm{d}l}{B}\int_0^{1/B}\frac{B\mathrm{d}\lambda}{\sqrt{1-\lambda B}}\,\overline{\widetilde{\phi}} = 2\oint\frac{\mathrm{d}l}{B}\,\widetilde{\phi} = 0 \tag{5.20}$$

by definition, we obtain the dispersion relation, accurate to the second order:

$$\Lambda = \frac{1+\langle k_\perp^2\lambda_D^2\rangle}{2} + \mathcal{O}\left(k_\perp^4\lambda_D^4\right)\ ,\quad \langle k_\perp^2\lambda_D^2\rangle = \frac{1}{\oint \mathrm{d}l/B}\oint\frac{\mathrm{d}l}{B}\,k_\perp^2\lambda_D^2 \tag{5.21}$$

In the crossing-point notation Eq. (5.9), this dispersion relation becomes

$$\frac{\overline{Z}_4}{2\zeta^3}\left(\nu-\frac{\tau}{c_\nu}\right) = \langle k_\perp^2\lambda_D^2\rangle. \tag{5.22}$$

It is instructive to find the asymptotes of this dispersion relation. For $\zeta\to\infty$

$$\nu+\tau = -\frac{4\zeta^4}{3}\left\langle k_\perp^2\lambda_D^2\right\rangle \iff \omega^2 = -\frac{3\,\tilde{\omega}_d^2}{\langle k_\perp^2\lambda_D^2\rangle}\left[\frac{\omega_T+\omega_n}{\tilde{\omega}_d}-5\right] \tag{5.23}$$

One sees that plasma is unstable if $\omega_T+\omega_n > 5\,\tilde{\omega}_d$, in agreement with Eq. (5.17). At the singularity line itself, $\omega = 0$ which contradicts the condition $\zeta \gg 1$, assumed above. This contradiction can be resolved taking higher-order terms in the plasma dispersion function into account. For this sake, we expand the plasma dispersion function (Fried &

Conte 1961) as

$$Z_0 = i\sqrt{\pi}e^{-\zeta^2} - \frac{1}{\sqrt{\pi}}\sum_{n=0}^{\infty}\frac{\Gamma(n+1/2)}{\zeta^{2n+1}} = \tag{5.24}$$
$$= i\sqrt{\pi}e^{-\zeta^2} - \frac{1}{\zeta} - \frac{1}{2\zeta^3} - \frac{3}{4\zeta^5} - \frac{15}{8\zeta^7} - \frac{105}{16\zeta^9} - \frac{945}{32\zeta^{11}}$$

This expansion leads to the dispersion relation:

$$\left\langle k_\perp^2\lambda_D^2\right\rangle = -\frac{3}{4\zeta^4}\left[(\tau+\nu) + \frac{35}{4\zeta^4}(3\tau+\nu)\right] \tag{5.25}$$

At the singularity line $\tau + \nu = 0$. Here, the dispersion relation degenerates to

$$\left\langle k_\perp^2\lambda_D^2\right\rangle = -\frac{105\tau}{8\zeta^8} \iff \omega^4 = -\tau\frac{210\,\tilde{\omega}_d^4}{\langle k_\perp^2\lambda_D^2\rangle} \tag{5.26}$$

Note that below the crossing point ($\tau < 0$), there is a single unstable root that is purely growing, whereas above the crossing point ($\tau > 0$), there are two unstable solutions with complex frequencies satisfying $\mathrm{Im}(\omega) = |\mathrm{Re}(\omega)|$.

In the opposite limit $\zeta \ll 1$, finite Debye length is less important. It only slightly shifts the stability boundary:

$$\nu - \tau = \left\langle k_\perp^2\lambda_D^2\right\rangle \iff \frac{\omega_n - \omega_T}{\tilde{\omega}_d} = 1 + \left\langle k_\perp^2\lambda_D^2\right\rangle \tag{5.27}$$

Summarizing, taking finite Debye length into account resolves the singularity in the growth rate appearing in Fig. 6. Instead one finds at the singularity boundary that the mode is purely growing ($\mathrm{Re}[\omega] = 0$) below the crossing point and has finite frequency and growth rate above the crossing point. The plasma is thus stable only if $\omega_n - \omega_T < \tilde{\omega}_d$ and $\omega_n + \omega_T < 5\,\tilde{\omega}_d$ are both satisfied (i. e. stability is only observed in the left triangular region of Fig. 6). This clarifies the role of the two stability lines identified by Helander (2014) and Helander & Connor (2016). Note that the point-dipole (Fig. 6) and Z-pinch (Fig. 5) stability diagrams are similar, with the main difference being simply the location of the crossing point of the stability lines.

6. Conclusions

In this paper, we have studied the drift-kinetic stability of a pair plasma, of equal positron and electron temperature and density, confined by a dipole magnetic field. The Z-pinch and point-dipole limits have both been considered, and the resulting dispersion relations have been derived, solved, and compared. We have found electrostatic instabilities in pure pair plasmas driven by the magnetic curvature, temperature and density gradients. In point-dipole geometry, when the Debye length is taken to be exactly zero, we have found that instabilities exist for the parameters in the domain bounded by Eqs. (5.6) and (5.7). Their growth rate decreases towards the stability boundary defined by Eq. (5.6), and increases towards the singularity boundary defined by Eq. (5.7). Visually, this is seen in Fig. 6 as an increase in the density of the contours of constant growth rate. The singularity can be resolved taking a small but finite Debye length into account. This is associated with a fluid-type mode that is absent if $k_\perp\lambda_D = 0$ exactly. In the Z-pinch limit, the stability diagram found is similar. With these observations, Figs. 6 and Fig. 5 describe rather thoroughly the drift-kinetic stability of pair plasmas in dipole geometry. We thereby clarify the role of the stability lines in parameter space, and conclude that

both density and temperature gradients drive instability. In Z-pinch geometry, we have also treated the Landau damping problem with a novel integration contour, and found exponential and algebraic damping solutions related to the drift particle motion. The existence of such unstable modes is a collective effect that can provide the background turbulence needed for an inward particle pinch (Isichenko *et al.* 1996). Such a pinch could be very helpful for pair-plasma creation. We plan to address this with a gyrokinetic code in future.

Acknowledgments We acknowledge Thomas Sunn Pedersen and PAX/APEX experiment team for their interest to our work.

REFERENCES

Biglari, H., Diamond, P. H. & Rosenbluth, M. N. 1989 Toroidal ion-pressure-gradient-driven drift instabilities and transport revisited. *Physics of Fluids B: Plasma Physics* **1** (1), 109–118.

Fried, B. D. & Conte, S. D. 1961 *The Plasma Dispersion Function*. New York: Academic Press.

Gradshteyn, I. S. & Ryzhik, I. M. 1980 *Table of integrals, series and products*. New York: Academic Press.

Helander, P. 2014 Microinstability of magnetically confined electron-positron plasmas. *Phys. Rev. Lett.* **113**, 135003+4.

Helander, P. 2017 Available energy and ground states of collisionless plasmas. *J. Plasma Phys.* **83**, 715830401+20.

Helander, P. & Connor, J. 2016 Gyrokinetic stability theory of electron-positron plasmas. *J. Plasma Phys.* **82**, 9058203+13.

Helander, P., Mishchenko, A., Kleiber, R. & Xanthopoulos, P. 2011 Oscillations of zonal flows in stellarators. *Plasma Phys Contr F* **53** (5), 054006.

Isichenko, M., Gruzinov, A., Diamond, P. & Yushmanov, P. 1996 Anomalous pinch effect and energy exchange in tokamaks. *Phys. Plasmas* **3**, 1916–1925.

Kessner, J. & Hastie, R. 2002 Electrostatic drift modes in a closed field line configuration. *Phys. Plasmas* **9**, 395–400.

Landau, L. & Lifshitz, E. 1960 *Electrodynamics of Continuous Media*. Pergamon Press.

Mishchenko, A., Zocco, A., Helander, P. & Koenies, A. 2017 Gyrokinetic stability of electron-positron-ion plasmas. *submitted to Journal of Plasma Physics* .

Pedersen, T., Boozer, A., Dorland, W., Kremer, J. & Schmitt, R. 2003 Prospects for the creation of positron-electron plasmas in a non-neutral stellarator. *J. Phys B: At. Mol. Opt. Phys.* **36**, 1029–1039.

Pedersen, T., Danielson, J., Hugenschmidt, C., Marx, G., Sarasola, X., Schauer, F., Schweikhard, L., Surko, C. & Winkler, E. 2012 Plans for the creation and studies of electronpositron plasmas in a stellarator. *New J. Phys.* **14**, 03510+13.

Saitoh, H., Stanja, J., Stenson, E., Hergenhahn, U., Niemann, H., Pedersen, T., Stoneking, M., Piochacz, C. & Hugenschmidt, C. 2015 Efficient injection of an intense positron beam into a dipole magnetic field. *New J. Phys.* **17**, 103038+9.

Simpson, J., Lane, J., Immer, C. & Youngquist, R. 2001 Simple analytic expressions for the magnetic field of a circular current loop. *NASA Technical Reports Server* .

Sugama, H. 1999 Damping of toroidal ion temperature gradient modes. *Phys. Plasmas* **6** (9), 3527–3535, arXiv: http://dx.doi.org/10.1063/1.873613.

Zocco, A. 2017 Slab magnetised non-relativistic low-beta electron-positron plasmas: collisionless heating, linear waves and reconnecting instabilities. *submitted to Journal of Plasma Physics* .